Abdallah Mohamed Abdelsalam, Ibrahim and Adam, Grain P. and Holliday, Derrick and Williams, Barry W. (2015) Three-phase ac-dc buck-boost converter with a reduced number of switches. IET Renewable Power Generation, 9 (5). pp. 494-502. ISSN 1752-1416 , http://dx.doi.org/10.1049/iet-rpg.2014.0077

A Three-Phase AC-DC Buck-Boost Converter with a Reduced Number of Switches

I. Abdelsalam[1,2], G.P. Adam[1]D. Holliday[1]and B.W. Williams[1]
Electronic and Electrical Engineering Department, University of Strathclyde, Glasgow, UK[1]
Electrical Power Department, Arab Academy for Science and Technology and Maritime Transport, Cairo, Egypt[2]

Abstract─ A single-switch, single-stage, three-phase, ac-dc buck-boost converter suitable for medium-voltage applications is proposed. Basic relations that govern steady-state converter operation are established, confirmed using PSCAD/EMTDC simulations, and substantiated experimentally. Simulation and experimental results establish that the proposed converter has good dynamic performance in buck and boost modes, with near unity input power factor.

Index Terms ─ ac-dc converter, buck-boost converter, medium-voltage applications, wind energy conversion systems.

I. INTRODUCTION

AC-DC conversion is widely used in applications such as power supplies for microelectronics, uninterruptible power supplies (UPS), battery chargers, wind energy conversion systems, household-electric appliances, dc-motor drives, and dc distributed systems [1-3]. Three-phase two-level ac-dc converters can be classified into three main categories, namely buck, boost and buck-boost converters. Buck converters [4-7] provide a dc output voltage lower that the peak of the ac supply voltage and reduce the number of power electronics switches to three, the number of diodes is increased and the converter requires a special firing technique. Reference [8] considers buck converters with isolation. Buck-boost converters can be classified into two categories: single-stage [9, 10] and double-stage [11, 12]. In [13, 14], a single-phase converter is used for each phase and a transformer provides isolation and matches the dc output of each converter. The boost converter is widely used in wind energy conversion systems [15-20] where a three-phase bridge rectifier and dc-dc converter are used to provide a stable dc voltage for a grid-connected inverter over the wide speed range of the input synchronous generator. The main disadvantages of these back-to-back converters are the need to pre-charge the dc side capacitor, and poor output short-circuits protection in case of the boost converter.

The proposed buck-boost converter consists of a three-phase bridge rectifier in series with a single switch as shown in Fig. 1(a). The single-phase version of the buck-boost converter was proposed and

incorrectly discarded [21] on the grounds that it could not be extended to a three-phase system. The three-phase version of the circuit was investigated, but disqualified it on the grounds of discontinuous and non-sinusoidal input current [22]. The buck-boost converter considered in this paper has been operated in a discontinuous mode using multi-resonance zero current switching [23, 24], but this approach is not suitable for high-power applications since a 25 kHz switching frequency is used. This paper reintroduces the three-phase buck-boost converter for medium-voltage and high-power applications where the switching frequency is less than 1.5 kHz. Additionally, this paper operates the presented buck-boost converter as a current source converter, where filter capacitance rated at 0.3pu to 0.6pu is required at the converter input for harmonic attenuation and to ensure sinusoidal input currents [25]. The buck-boost converter under investigation offers the following features:

- Buck and boost capability in a single stage with a minimum switch count.
- Stable dc voltage output in buck and boost modes, making it applicable as a front-end converter for grid-connected current and voltage source converters, with black-start and shutdown capabilities.

This paper is organized as follows: Section II describes the operating principle of the proposed three-phase ac-dc buck-boost converter, and establishes the basic equations that govern its steady-state operation, control loop and filter design. Section III uses simulation results obtained from PSCAD/EMTDC to demonstrate the technical feasibility of the presented ac-dc buck-boost converter. Section IV presents experimental results from a prototype ac-dc buck-boost converter that validates the simulation results presented in Section III. Scalability of the ac-dc buck-boost converter to medium-voltage multi-megawatt level is demonstrated in Section V. Conclusions and major findings are highlighted in Section VI.

II. PROPOSED THREE-PHASE BUCK-BOOST BRIDGE

a. Circuit Description

Fig.1 (a) shows that the three-phase ac-dc buck-boost converter being investigated consists of a three-phase L-C filter followed by a three-phase bridge rectifier, with a series switch S placed between the bridge and the dc side inductor L_{dc}. Switch S adjusts the dc output load voltage by controlling the average current flow in inductor L_{dc}, and hence controls the power flow between the ac and dc sides. The three-phase buck-boost converter has seven operational modes, six of which are conducting modes whilst the seventh is an intervening freewheeling mode. The conducting modes occur when switch S is turned on allowing the ac current to be converted to dc when energizing inductor L_{dc}. During this period, the dc inductor current I_L increases and blocking diode D_{bd} is reverse biased. The dc side capacitor C_{dc} thus discharges to supply the load. The different conducting modes are defined by the conduction sequence of the three-phase bridge rectifier diodes, and are shown in Table 1. Bridge diode conduction Mode1 is shown as an example in Fig.1 (b). The freewheeling mode (Mode 7) occurs when switch S is turned off, allowing dc inductor current I_L to decrease whilst charging the dc side capacitor C_{dc} and supplying the load, as shown in Fig.1(c).

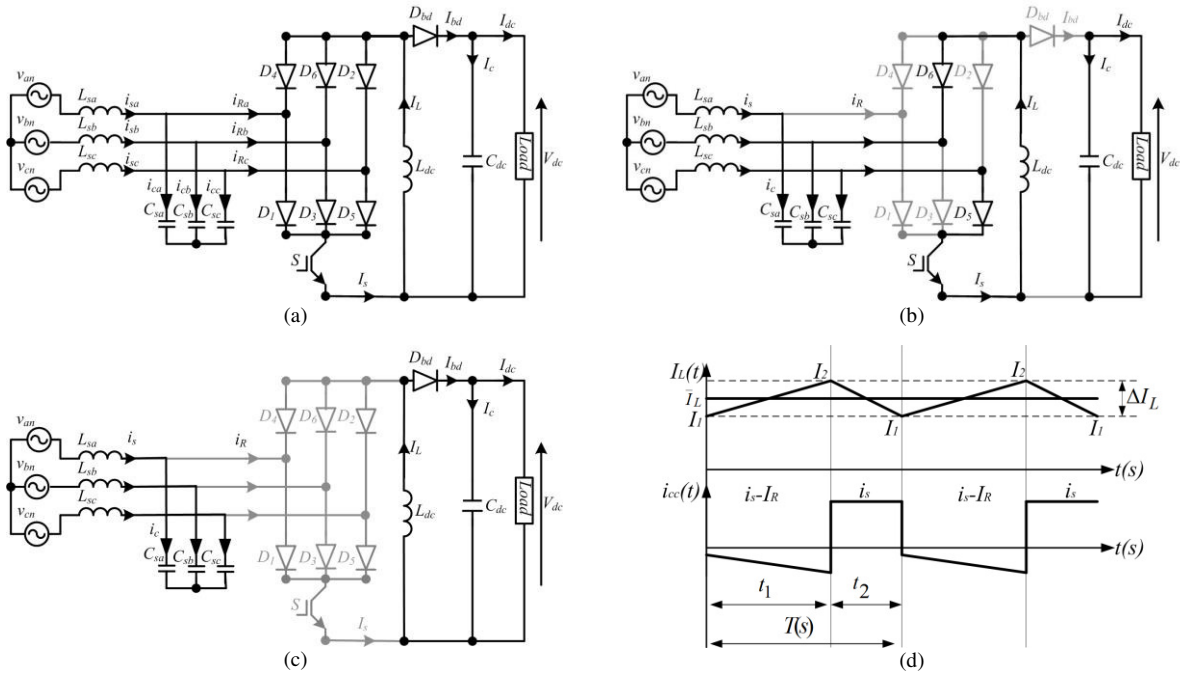

Fig.1:Proposed buck-boost converter and illustration of its operation (a) topology, (b)Mode 1 operation: conduction, (c)Mode 7 operations: freewheeling, and (d) inductor current I_L and ac side filter current during a full Mode 1 switching cycle.

Table 1: Proposed three-phase buck-boost converter conduction modes

	Operating Mode					
	Mode 1	Mode 2	Mode 3	Mode 4	Mode 5	Mode 6
Conduction period ωt	0°-60°	60°-120°	120°-180°	180°-240°	240°-300°	300°-360°
Lower active diode	D_5	D_1	D_1	D_3	D_3	D_5
Upper active diode	D_6	D_6	D_2	D_2	D_4	D_4

In Mode 1, diodes D_5 and D_6 conduct since they experience the largest line-to-line voltage, hence the three-phase bridge dc output voltage is equal to the instantaneous ac side capacitor line-to-line voltage vc_{cb}, i.e. the voltage across capacitor C_{sc} with respect to that across capacitor C_{sb}. When the switch S is in the 'on' state, the ac side capacitor C_{sc} discharges by changing its current direction to supply dc side inductor L_{dc}, where the dc side inductor current I_L equals the sum of the ac side filter capacitor current i_{cc} and supply current i_{sc}. When switch S is in the 'off' state, the ac side capacitor C_{sc} starts to charge and its current i_{cc} is equal to supply current i_{sc}, as shown in Fig.1(c) and (d). The following assumptions are made when deriving an expression for the dc output voltage, V_{dc}.

1. The switching period is $T=t_1+t_2$, such that a conduction mode occurs during $0 \le t \le t_1$ and the freewheeling mode occurs during $t_1 \le t \le t_2$, as illustrated in Fig.1(d).
2. The ac side capacitor operates in a continuous conduction mode.
3. The three-phase bridge average output voltage is $\frac{-3\sqrt{3}}{\pi} V_{Cm}$, where V_{Cm} is the peak fundamental phase voltage across the ac side capacitors. The negative sign reflects the inversion of the bridge output voltage with respect to the load ground.
4. The dc side inductor current is continuous, increasing linearly from I_1 to I_2 during $0 \le t \le t_1$ and decreasing linearly from I_2 to I_1 during $t_1 \le t \le t_2$, so that $\Delta I_L = I_2 - I_1$, as shown in Fig.1(d).
5. The ac side current is sinusoidal and is in ac steady-state during each switching period.

Switching utilizes a combination of natural and forced commutation of the diodes, and a self-commutated switch to achieve balanced current sharing between the diodes. In Mode 1, the voltage across dc side inductor L_{dc} equals the instantaneous value of v_{Ccb}. The differential equations describing operation during conduction Mode 1 are:

$$\frac{dI_L}{dt} = \frac{v_{Ccb}}{L_{dc}} \tag{1}$$

$$\frac{dV_{dc}}{dt} = \frac{-I_{dc}}{C_{dc}} \tag{2}$$

$$i_{sc} = i_{cc} + I_s \tag{3}$$

where I_s is the instantaneous switch (IGBT) current, i_{cc} is the current in the ac filter capacitor of phase 'c', i_{sc} is phase 'c' supply current, I_{dc} is the instantaneous dc output (load) current, V_{dc} is the dc load voltage, vc_{cb} is the line-to-line voltage across the ac filter capacitors connected between phases 'b' and 'c', and I_L is inductor current.

In freewheeling Mode 7, the dc side equations are:

$$\frac{dI_L}{dt} = \frac{-V_{dc}}{L_{dc}} \tag{4}$$

$$\frac{dv_{dc}}{dt} = \frac{I_L - I_{dc}}{C_{dc}} \tag{5}$$

In this mode, the rectifier input currents i_{Ra}, i_{Rb} and i_{Rc} are zero. Thus equation (3) becomes:

$$i_{sc} = i_{cc} \tag{6}$$

For phase 'c', the ac filter current is:

$$i_{cc} = C\frac{dv_{Cc}}{dt} \tag{7}$$

For the conducting modes, equation (1) becomes:

$$\Delta I_L = \frac{3\sqrt{3}}{\pi}\frac{t_1 V_{Cm}}{L_{dc}} \tag{8}$$

Similarly, equation (4) in the freewheeling mode becomes:

$$\Delta I_L = \frac{-t_2 V_{dc}}{L_{dc}} \tag{9}$$

From (8) and (9):

$$\frac{3\sqrt{3}}{\pi}\frac{t_1 V_{Cm}}{L_{dc}} = \frac{t_2 V_{dc}}{L_{dc}} \tag{10}$$

$$V_{dc} = \frac{3\sqrt{3}}{\pi}\frac{\delta}{1-\delta}V_{Cm} \tag{11}$$

Where $\delta=t_1/T$ is the switch on-state duty cycle such that $0\leq\delta\leq1$.

Since dc side capacitor voltage balance necessitates that the average capacitor current over one or a number of consecutive switching cycles is zero ($\bar{I}_c=0$), the relationship between the average inductor current $\bar{I}_L$ and the average load current $\bar{I}_{dc}$ is:

$$\bar{I}_c = \frac{1}{T}\left(\int_0^{\delta T}(-\bar{I}_{dc})dt + \int_{\delta T}^{T}(\bar{I}_L - \bar{I}_{dc})dt\right) = 0 \tag{12}$$

$$\bar{I}_{dc} = (1-\delta)\bar{I}_L \tag{13}$$

Therefore, for a resistive load, the average dc output voltage $\bar{V}_{dc}$ can be expressed in terms of average inductor current $\bar{I}_L$.

$$\bar{V}_{dc} = (1-\delta)R_{dc}\bar{I}_L \tag{14}$$

Since the switch current I_s is equals to the inductance current I_L in the conducting modes, relation between the average switch current $\bar{I}_s$ and the average inductor current $\bar{I}_L$ is:

$$\bar{I}_s = \delta\bar{I}_L \tag{15}$$

The relation between average switch current $\bar{I}_s$ and the average output current $\bar{I}_{dc}$ can drive by substituting equation (13) in (15):

$$\bar{I}_s = \frac{\delta}{1-\delta}\bar{I}_{dc} \tag{16}$$

Assuming lossless conversion, power balance dictates that power into the converter equals the dc output power:

$$\frac{3}{2}i_{Rm\_fund}V_{cm} = V_{dc}I_{dc} \tag{17}$$

Where: i_{Rm_fund} is the peak fundamental converter input current. Substituting (11) into (17) gives:

$$i_{Rm\_fund} = \frac{2\sqrt{3}}{\pi}\frac{\delta}{1-\delta}\bar{I}_{dc} \tag{18}$$

The rms current in switch S can be calculated as [26]:

$$I_{s\_rms} = \bar{I}_L\sqrt{\delta}\sqrt{1+\frac{1}{3}\left(\frac{\Delta I_L}{\frac{2}{\bar{I}_L}}\right)^2} \tag{19}$$

Equation (19) can used to calculate the per-phase rms converter input current i_{R_rms}:

$$i_{R-rms} = \sqrt{\frac{2}{3}}I_{s\_rms} = \sqrt{\frac{2}{3}}\bar{I}_L\sqrt{\delta}\sqrt{1+\frac{1}{3}\left(\frac{\Delta I_L}{\frac{2}{\bar{I}_L}}\right)^2} \tag{20}$$

To facilitate analysis of the rectifier input current, the dc side inductance L_{dc} is assumed sufficiently large so that the dc side inductor current is constant (ripple free) and equals $\bar{I}_L$. Fig.2 shows rectifier input current during one fundamental cycle, and shows that this three-phase buck-boost converter operates with a constant duty cycle. A triangular carrier is used to ensure good harmonic performance, with the current pulses centred within each carrier period.

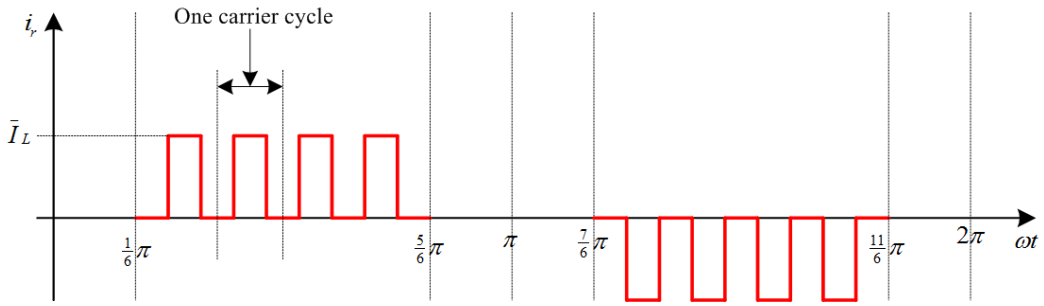

Fig.2: Rectifier input current during one carrier cycle.

The spectrum of the rectifier input current i_R can be obtained using the double Fourier series in complex form [27]:

$$i_{R(m,n)} = \frac{1}{2\pi^2}\left[\int_{\frac{\pi}{6}-\delta\pi}^{\frac{5\pi}{6}\ \delta\pi}\int I_L e^{j(mx+ny)}dxdy - \int_{\frac{7\pi}{6}-\delta\pi}^{\frac{11\pi}{6}\ \delta\pi}\int I_L e^{j(mx+ny)}dxdy\right] \quad (21)$$

Where: $y=\omega_0 t$ and $x=\omega_c t$, ω_0 and ω_c respectively represent fundamental and carrier frequencies in rad/s, and where m and n respectively are the orders of the carrier and baseband component harmonics.

The baseband harmonics of the rectifier input current i_R are computed by setting m=0 in (21), yielding:

$$i_{R(0,n)} = A_{0n} + jB_{0n} = \frac{j2\sqrt{3}\delta\,\bar{I}_L}{n\pi} \quad (22)$$

Equation (22) is valid for all n that represent odd and non-triplen harmonics; otherwise $C_{0n}=0$, meaning that $A_{0n}=0$ and $B_{0n}=\frac{2\sqrt{3}\delta\,\bar{I}_L}{n\pi}$. The peak value of the rectifier input fundamental component i_{Rm_fund} is obtained with n=1, so that:

$$i_{Rm\_fund} = \frac{2\sqrt{3}\delta\,\bar{I}_L}{\pi} = \frac{2\sqrt{3}}{\pi}\frac{\delta}{1-\delta}\bar{I}_{dc} \quad (23)$$

The peak fundamental current obtained from the double Fourier series (23) is the same as that obtained from the power balance equation (18). This validates the input current analysis presented.

The carrier frequency harmonic components are obtained by setting n=0 in(21), yielding:

$$i_{R(m,0)} = A_{m0} + jB_{m0} = \frac{4\bar{I}_L}{3m\pi}\sin(\delta m\pi) \quad (24)$$

From (24), $A_{m0} = \frac{4\bar{I}_L}{3m\pi}$ and $B_{m0}=0$. The peaks of the 1st and 2nd carrier frequency components can be obtained by setting m=1 and 2 respectively.

The sideband harmonics are obtained by computing (21) for non-zero m and n as:

$$i_{R(m,n)} = A_{mn} + jB_{mn} = \frac{j4\bar{I}_L}{nm\pi^2}\sin(\delta m\pi)\sin\left(\frac{1}{3}n\pi\right)e^{j\frac{1}{2}\pi(n+1)} \quad (25)$$

From (25), $A_{mn}=0$ and $B_{mn} = \frac{4\bar{I}_L}{nm\pi^2}\sin(\delta m\pi)\sin\left(\frac{1}{3}n\pi\right)e^{j\frac{1}{2}\pi(n+1)}$, and from the double Fourier series, the rectifier input current expressions are:

$$i_{R(m,n)} = \frac{1}{2}A_{00} + \sum_{n=1}^{\infty}(A_{0n}\cos n\omega_0 t + B_{0n}\sin n\omega_0 t) + \sum_{m=1}^{\infty}(A_{m0}\cos m\omega_c t + B_{m0}\sin m\omega_c t) + \sum_{m=1}^{\infty}\sum_{n=-\infty}^{\infty}(A_{mn}\cos((m\omega_c + n\omega_0)t) + B_{mn}\sin((m\omega_c + n\omega_0)t)) \quad (26)$$

$$i_{R(m,n)} = \frac{2\sqrt{3}\delta\bar{I}_L}{\pi}\sum_{n=1}^{\infty}\frac{1}{n}\sin n\omega_0 t + \frac{4\bar{I}_L}{3\pi}\sum_{m=1}^{\infty}\frac{1}{m}\sin(\delta m\pi)\cos m\omega_c t + \frac{4\bar{I}_L}{\pi^2}\sum_{m=1}^{\infty}\sum_{n=-\infty}^{\infty}\frac{1}{mn}\sin(\delta m\pi)\sin\left(\frac{1}{3}n\pi\right)e^{j\frac{1}{2}\pi(n+1)}\sin((m\omega_c + n\omega_0)t) \quad (27)$$

Equation (27) provides a theoretical solution for interpreting the ac harmonic distribution of the converter under investigation, including basebands, carrier frequency, and sidebands harmonics. Also, equation (27) assists the filter design as it provides information about the location of the dominant low-order and switching frequencies to be eliminated.

b. Control Stage

The proposed buck-boost converter gives a stable output dc voltage using the simple control structure in Fig.3, which consists of an outer voltage control loop and an inner current control loop. In the voltage control loop, the reference dc voltage V_{dc_ref} is subtracted from the load voltage V_{dc_fb}, and then the voltage error is input to a PI controller, which generates the output dc current reference signal I_{dc_ref}. A current limiter is used to provide overload protection. I_{dc_ref} is the input to the current control loop and is subtracted from the load current. The resulting error is input to a PI controller, whose output is compared with a triangular carrier wave to provide the gating signal required to control the buck-boost converter switch.

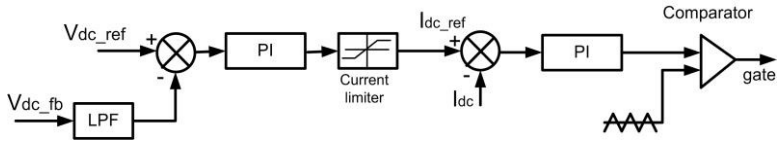

Fig.3: Three-phase buck-boost converter control circuit.

c. Filter Design

Like the rectifier with constant current load, the phase current conduction period of the buck-boost converter is $2\pi/3$ radians per half-cycle. The design of the ac side LC filter depends on several factors, such as the rectifier switching frequency (which is between 512Hz and1.2kHz for medium-power applications), LC resonant mode, required line current total harmonic distortion (THD), and input power factor. Equation (22) can be used to show that the converter input current contains high amounts of the 5^{th} and the 7^{th} harmonics. The cut-off frequency of the ac side filter is therefore selected to be 2.5 times greater than the supply frequency f (50Hz in this case) and the input filter capacitances 0.33pu, which is within the normal range for capacitance in high-power PWM-current source rectifiers that use a low switching frequency [28]. Simulation results for different operating conditions show that for acceptable supply current THD; the ac filter cut-off frequency must be 2.4f. On this basis, the ac side filter inductance L_S can therefore be calculated as shown in (28) and (31):

$$2.4\omega_B = \frac{1}{\sqrt{L_s C_s}} \tag{28}$$

$$L_s = \frac{1}{5.76\omega_B{}^2 C_s} \tag{29}$$

Where: ω_B is the base frequency in rad/s, C_S is the ac side filter capacitance, base capacitance $C_B = \frac{1}{\omega_B Z_B}$, base inductance $L_B = \frac{Z_B}{\omega_B}$ and Z_B is the base impedance [25].

$$L_s = \frac{1}{5.76\omega_B{}^2 (\frac{0.33}{\omega_B Z_B})} = \frac{Z_B}{1.9\omega_B} = 0.53 L_B \tag{30}$$

Equations (31) and (32) express the ac side filter parameters based on rated line-to-line voltage V_{LL} and desired converter input power P in a star configuration, while equation (33) specifies the filter capacitance C_s in the delta connection case.

$$L_s = 0.53 \frac{V_{LL}^2}{2\pi f P} \tag{31}$$

$$C_s = 0.33 \frac{P}{2\pi f V_{LL}^2} \tag{32}$$

$$C_s = 0.11 \frac{P}{2\pi f V_{LL}^2} \tag{33}$$

d. Power Factor

Based on simulation and experimental results obtained under different operating conditions, it has been shown that the proposed buck-boost converter power factor profile depends on the converter input power, and is independent of operating mode (buck or boost).Fig.4 shows the power factor profile at different load conditions, using the filter values based on equations (31) and (32). The input power factor of the proposed buck-boost converter varies in the narrow range between 0.98 and 1when the converter input power is varied between 0.8pu and 1.2pu. Between input power of 0.7pu and 0.8pu, power factor varies between0.95 and 0.98. Below this operating range, the converter input power factor decreases to 0.85 at 0.5 pu of rated input power.

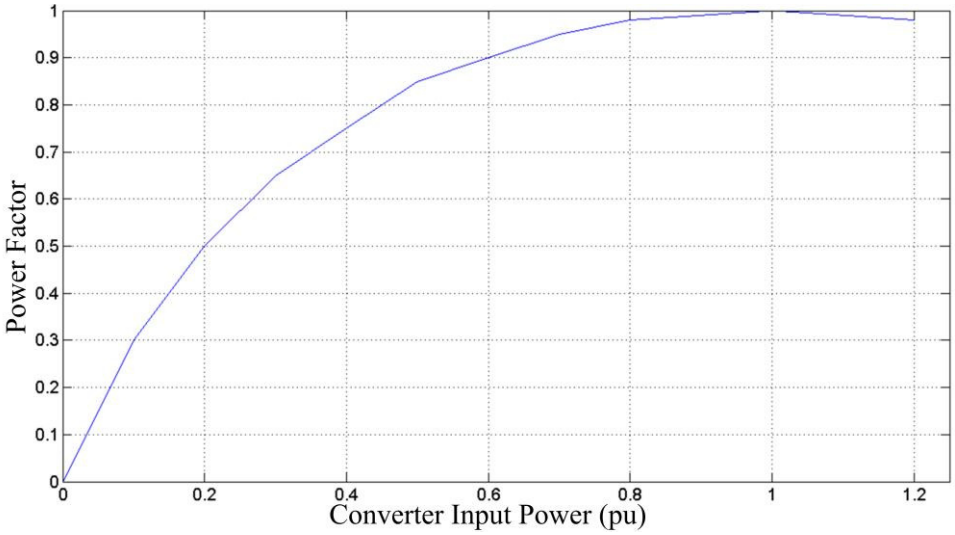

Fig.4 Power factor profile of the proposed buck-boost converter.

III. SIMULATION VALIDATION

This section presents simulation results of the proposed buck-boost converter, using the PSCAD/EMTDC environment, with the three-phase converter operating in buck and boost modes. The converter parameters used in both the simulations and experimental validation are listed in Table 2.

Table 2Proposed three-phase converter buck-boost parameters

Parameter	Value
Rated input power	1800W
Input supply line-to-line voltage	75V

Supply frequency	50Hz
AC side per phase filter capacitance (delta-connected)	115μF
AC side per phase filter inductance	5.7mH
DC side inductance	5mH
DC side capacitance	3300μF
PWM switching frequency	1.2kHz
Load resistance	26Ω

Experimentation and simulation are both conducted at the rated input power of P =1800W. From equation (31) the ac side inductance is 5.3mH (experimentally, 5.7 inductance are used due to their availability), while from equation (33), the ac side filter capacitance is 112μF (experimentally, 115 μF capacitors are used due to their availability).

The reference dc voltage V_{dc_ref} is passed through a 1Hz low-pass filter to ramp any step change in the dc reference voltage V_{dc_ref} .This ensures controlled charging of the bulky dc side capacitor filter, avoiding the need for a capacitor pre-charge circuit. The dc voltage reference is initially V_{dc_ref}=154V. At t=3s, the reference is stepped to V_{dc_ref}=174V. At t=6s, the reference is stepped to V_{dc_ref}=204V. These values correspond to 0.55pu, 0.72pu and 1pu rated input power, respectively.

Fig.5 shows simulation results when the converter is operated from a 50Hz three-phase ac supply. Fig.5(a) shows the converter dc output voltage, where the converter is able to provide stable dc voltage with soft start-up. Fig.5(b) shows the supply current, which increases smoothly without overshoot or oscillation. Fig.5(c) shows the active input power at each output voltage. Fig.5(d) shows a detailed view of the three-phase supply current and phase-a voltage at V_{dc_ref} =174V, where the supply current has a THD=4.03% and a power factor=0.956. Fig.5(e) shows a detailed view of the three-phase supply current and phase-a voltage at V_{dc_ref}= 204V where THD=4.4% and power factor=0.999. The results in Fig.5 establish that the proposed three-phase buck-boost converter can provide high-quality sinusoidal input current with a power factor dependant on the rated power of the converter, as mentioned in Section II and as shown in Fig.4.

Fig.6 shows the harmonics spectra of the rectifier pre-filter input current $i_R(t)$ and supply current $i_s(t)$ when the proposed buck-boost regulates its dc link voltage (V_{dc}) at 174V. Under this operating condition, the average load current is 6.7A dc, and duty cycle (δ) provided by the current controller is about 0.6. According to equations (18) and (23) the expected peak fundamental rectifier input current

is 11.08A when δ =0.6, Fig.6(a) shows harmonics spectrum of the rectifier input current and its peak value are similar to the expected theoretical values. Fig.6(b) shows that the proposed filters design is able attenuates the harmonic content in the pre-filter rectifier current over wide operating range.

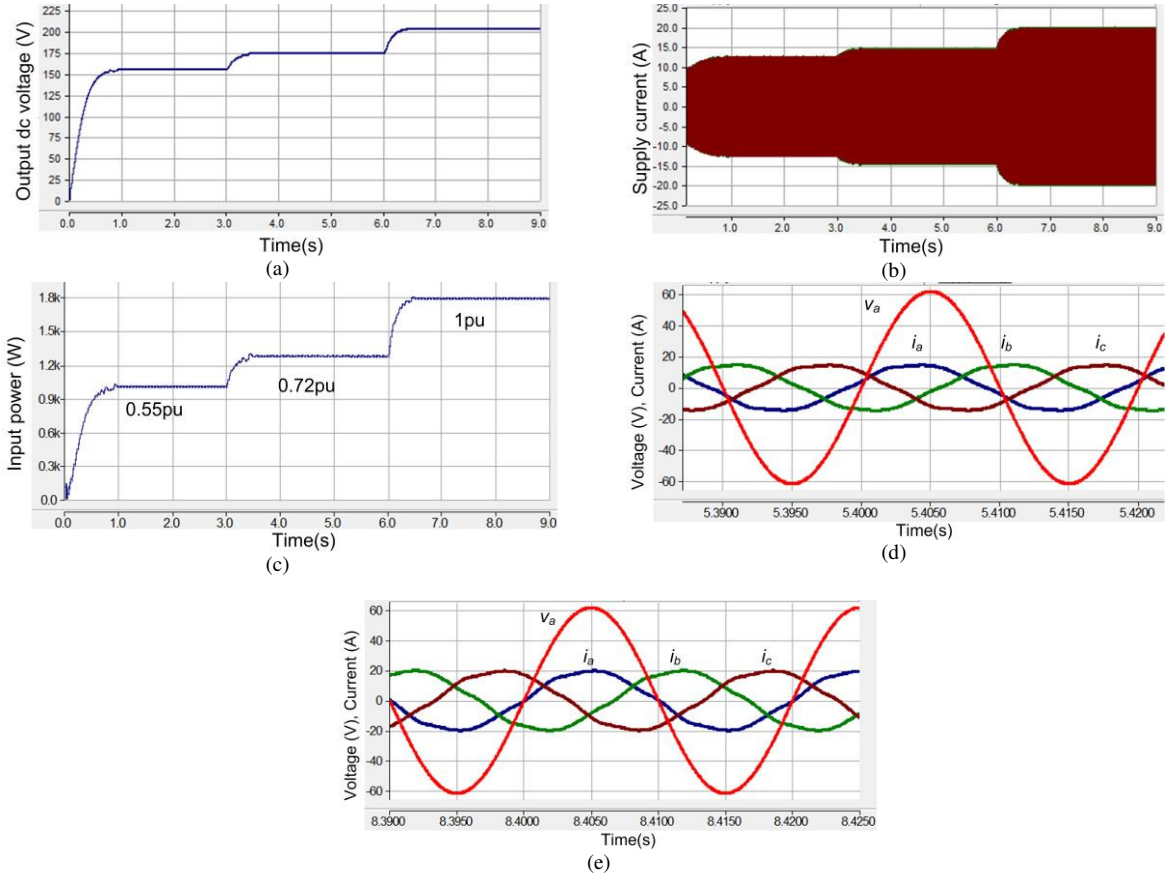

Fig.5: Simulation of the three-phase buck-boost converter during buck and boost operation modes, (a) output dc voltage, (b) input supply current, (c) input active power profile, (d) input supply three-phase currents and phase-a voltage at V_{dc_ref}=174V, and (e) input supply three-phase currents and phase-a voltage at V_{dc_ref}=204V

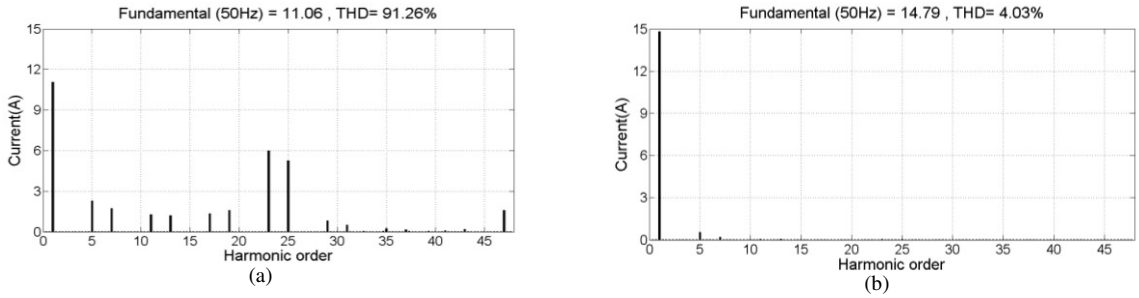

Fig.6 Waveforms show the rectifier input current and the supply current harmonics spectrum at V_{dc_ref} =174V.(a) Rectifier input current harmonics spectrum, and (b) Supply input current harmonics spectrum.

IV. EXPERIMENTAL VALIDATION

Experimental results for a 1.8kW version of the proposed three-phase buck-boost converter are presented in Fig.7 and Fig.8 to substantiate the theoretical discussion in Section II, and to confirm the

simulations presented in Section III. The parameters used for both simulation and experimental validation of the proposed buck-boost converter are listed in Table 2.

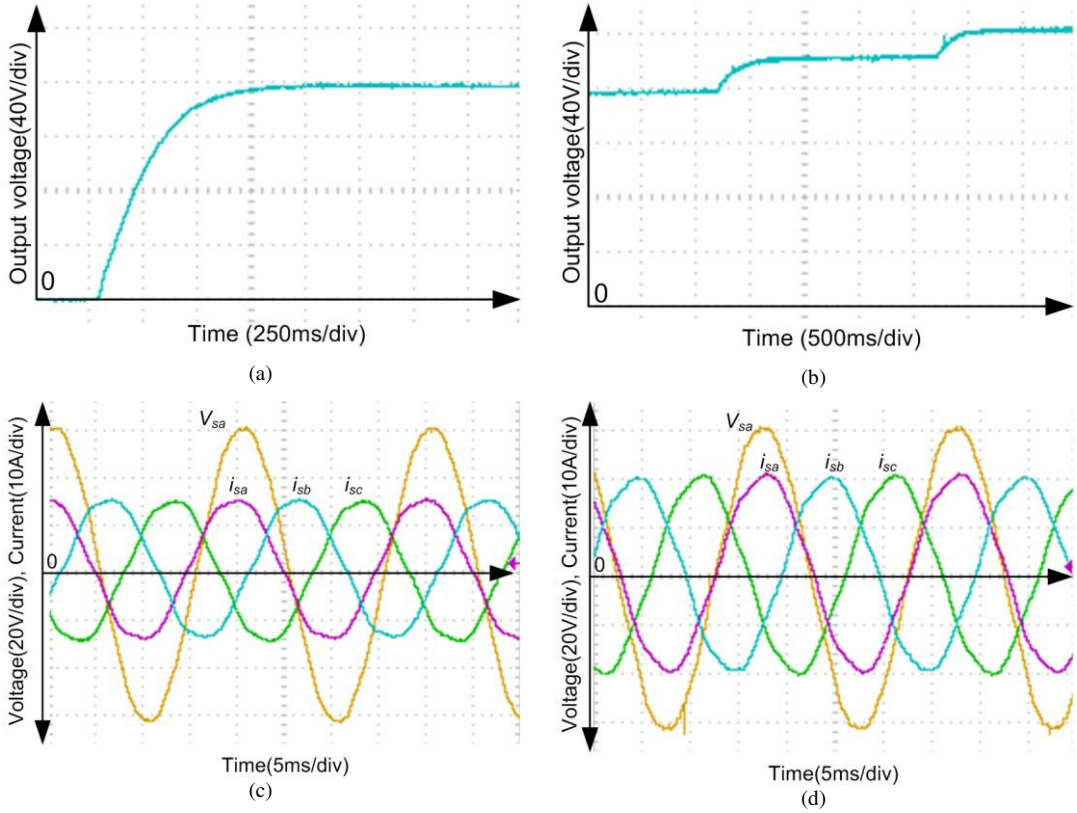

Fig.7: Experimental waveforms for the 2kW prototype three-phase buck-boost converter demonstrating its practical viability, (a) output dc voltage during start-up from zero to 154V, (b) output dc voltage during transitions from 154V to 174V and from 174V to 204V, (c) detailed view of the three-phase supply currents and phase-a voltage at 0.72pu of rated input power, and (d) detailed view of the three-phase supply currents and phase-a voltage at 1pu of rated input power.

Fig.7(a) shows the output voltage during start-up from zero to 154V (buck mode), where the voltage build-up is stable and gradual. Fig.7(b) shows dc output voltage during steady state, and during the transitions from 154V to 174V and from 174V to 204V (boost modes). Fig.7(c) and (d) show the three-phase input currents and phase-a voltages, where V_{dc_ref} =174V and V_{dc_ref} =204V respectively. The input currents are continuous and sinusoidal with limited distortion and near unity power factor, as with the simulations shown in Section III. These results establish that the presented ac-dc buck-boost converter could be used as an interfacing converter for permanent magnets wind-turbine generators, without the risk of pulsating torque that results with diode bridge rectification.

Fig.8(a) shows dc side inductor current I_L, dc load current I_{dc}, and switch S and diode D_{bd} currents I_s and I_{bd} respectively. From Fig.8(a), the current I_L in the dc side inductance increases during the 'on' period and is equal to the switch current I_S, while during the 'off' period the current in the inductor reduces and is equal to the blocking diode current I_{bd}. The voltage stresses across the dc side inductor V_L, switch V_S and diode V_{bd} are shown in Fig.8(b), from which it can be seen that the inductor voltage V_L is equal to the supply voltage during the 'on' period and equal to the output dc voltage during the 'off' period. The maximum switch voltage stress ($V_{S\text{-}max}$) is the sum of the peak line voltage across the ac side capacitors and the dc output voltage during the off-period. The maximum voltage stress on the blocking diode ($V_{bd\text{-}max}$) is the sum of the peak line voltage across the ac side capacitors and the dc output voltage during the on-period.

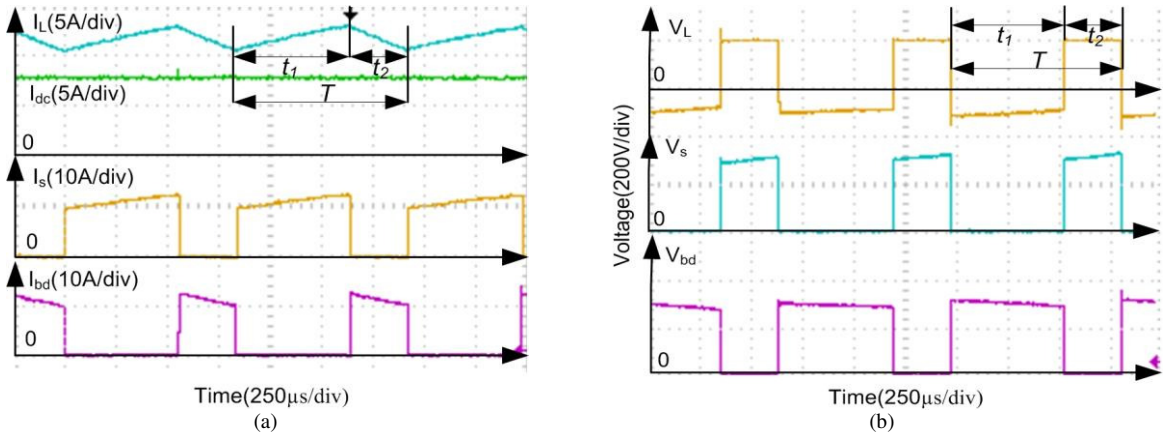

Fig.8: Experimental voltage and current waveforms for the dc side inductor, blocking diode and switch at the largest output voltage V_{dc_ref}=204V, (a) dc inductor currents, output dc current, bridge rectifier output current, and dc blocking diode(D_{bd}) current, and (b) Voltage across dc side inductor, semiconductor switch S and blocking diode D_{bd}.

The results in Fig.8 aid in the determination of the current and voltage ratings of the dc side inductor L_{dc}, switch S, and blocking diode D_{bd}. The results presented in Fig.5 to Fig.8 establish that the proposed buck-boost converter is a viable candidate for high-power, medium-voltage ac-dc applications. Table 3, which summarises the converter's performance, shows that the supply current has low THD and high power factor over a wide operating range. At 98%, the efficiency of the proposed buck-boost converter is good. The 2% power loss is due to:

- dc and ac copper resistance losses in the dc side inductance.
- Semiconductor power losses, from the series connection of two diodes and an IGBT switch.

- Forward voltage drop across the power diodes (2.3V at 25°C), and IGBT forward voltage V_{CE} (1.95V at 25°C): these would be less significant at higher supply voltages.

Overall system efficiency is also reduced due losses in the ac side inductor.

Table 3: Summary of the overall performance of the proposal buck-boost converter.

Input Power (W)	Input Power (pu)	Power Factor	Output dc Voltage (V)	Output dc Power (W)	Overall Efficiency (%)	Supply Current THD (%)	Converter Input Power (W)	Converter Efficiency (%)
1800	1	0.996	204	1606.7	0.89	3.94	1625W	0.985
1300	0.722	0.955	174	1164	0.895	4.14	1185W	0.98
1005	0.55	0.873	154	915.6	0.91	3.87	927W	0.987

V. CONVERTER SCALABILITY

To investigate the potential applicability of the of the proposed buck-boost converter in high-power, medium-voltage applications, a 2.5MW version of the proposed converter connected to a 3.3kV line-to-line ac supply, with parameters listed in Table 4, was designed and simulated. The results of the simulation are displayed in Fig.9. In Fig.9(a), the dc output voltage is ramped from 0 to 6.6kV_{dc}. The output dc voltage ripple in the steady state is minimal, being less than 1.5% of the output voltage as shown in the insert in Fig.9(a). Fig.9(b) shows that the converter draws sinusoidal supply current with low distortion and high power factor. Finally Fig.9(c) shows the change in the output power, from zero to maximum power. The required voltage rating of switch S, for a 3.3kV input line voltage and 6.6kV output dc voltage, is 11.66kV as shown in Fig.9(d), implying series device connection.

Table 4: Proposed buck-boost medium-voltage system parameters.

Medium-Voltage System Parameters	Rating
Rated power	2.5MW
Input supply line-to-line voltage	3.3kV
Supply frequency	50Hz
AC side per phase filter capacitance (delta-connected)	80μF
AC side per phase filter inductance	7.7mH
DC side inductance	2.8mH
DC side capacitance	2200μF
PWM switching frequency	1.2kHz
Load resistance	17.4Ω

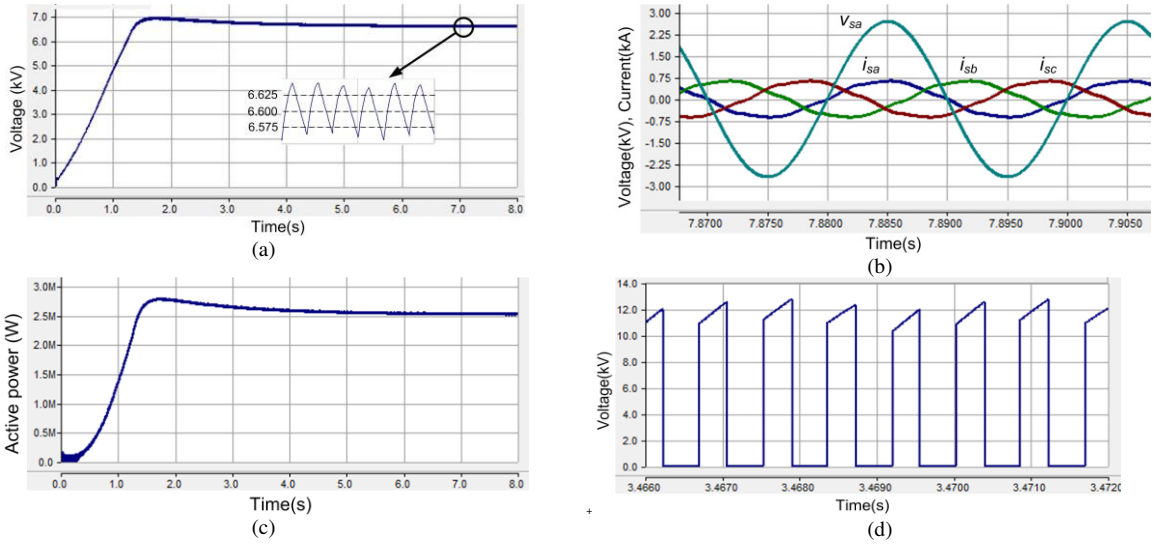

Fig.9:Simulation waveforms for the 2.5MW system, illustrating scalability of the proposed buck-boost converter, (a) output dc voltage,(b) input supply current (multiplied by 2) and phase-a voltage in steady state, (c) output power, and (d) switch voltage stress.

VI. CONCLUSION

A three-phase ac-dc buck-boost converter, that operates in continues conduction mode with relatively low switching frequency is proposed and investigated. The distinct feature of the proposed converter is that it achieves buck and boost operation in a single-stage, with adjustable dc output voltage in both modes. The ac side filter design ensures high power factor at rated power, and low input current THD. The theory, simulations, and experimental results presented establish that the proposed ac-dc buck-boost converter is viable for medium-voltage, high-power, ac-dc conversion applications, including grid interfacing of wind energy systems.

VII. REFERENCES

[1] J. W. Kolar and T. Friedli, "The Essence of Three-Phase PFC Rectifier Systems—Part I," Power Electronics, IEEE Transactions on, vol. 28, pp. 176-198, 2013.

[2] K. Shu-Kong and D. D. C. Lu, "A High Step-Down Transformerless Single-Stage Single-Switch AC/DC Converter," Power Electronics, IEEE Transactions on, vol. 28, pp. 36-45, 2013.

[3] H. S. Kim, M. H. Ryu, J. W. Baek, and J. H. Jung, "High-Efficiency Isolated Bidirectional AC-DC Converter for a DC Distribution System," Power Electronics, IEEE Transactions on, vol. 28, pp. 1642-1654, 2013.

[4] T. Nussbaumer, M. L. Heldwein, G. Guanghai, S. D. Round, and J. W. Kolar, "Comparison of Prediction Techniques to Compensate Time Delays Caused by Digital Control of a Three-Phase Buck-Type PWM Rectifier System," Industrial Electronics, IEEE Transactions on, vol. 55, pp. 791-799, 2008.

[5] M. L. Heldwein, T. Nussbaumer, and J. W. Kolar, "Common mode modelling and filter design for a three-phase buck-type pulse width modulated rectifier system," Power Electronics, IET, vol. 3, pp. 209-218, 2010.

[6] S. K. Bassan, D. S. Wijeratne, and G. Moschopoulos, "A Three-Phase Reduced-Switch High-Power-Factor Buck-Type Converter," Power Electronics, IEEE Transactions on, vol. 25, pp. 2772-2785, 2010.
[7] N. Krihely, M. A. Slonim, and S. Ben-Yaakov, "Transient and steady-state analysis of three-phase pwm buck rectifier," Power Electronics, IET, vol. 5, pp. 1764-1775, 2012.
[8] A. A. Badin and I. Barbi, "Unity Power Factor Isolated Three-Phase Rectifier With Two Single-Phase Buck Rectifiers Based on the Scott Transformer," Power Electronics, IEEE Transactions on, vol. 26, pp. 2688-2696, 2011.
[9] I. Barbi and F. A. B. Batista, "Space Vector Modulation for Two-Level Unidirectional PWM Rectifiers," Power Electronics, IEEE Transactions on, vol. 25, pp. 178-187, 2010.
[10] D. Wijeratne and G. Moschopoulos, "A novel three-phase buck-boost ac-dc converter," presented at the Applied Power Electronics Conference and Exposition (APEC), 2011 Twenty-Sixth Annual IEEE, 2011.
[11] Y. Lung-Sheng, L. Tsorng-Juu, and C. Jiann-Fuh, "Analysis and Design of a Novel Three-Phase AC–DC Buck-Boost Converter," Power Electronics, IEEE Transactions on, vol. 23, pp. 707-714, 2008.
[12] T. Nussbaumer, G. Guanghai, M. L. Heldwein, and J. W. Kolar, "Modeling and Robust Control of a Three-Phase Buck+Boost PWM Rectifier (VRX-4)," Industry Applications, IEEE Transactions on, vol. 44, pp. 650-662, 2008.
[13] B. Tamyurek and D. A. Torrey, "A Three-Phase Unity Power Factor Single-Stage AC–DC Converter Based on an Interleaved Flyback Topology," Power Electronics, IEEE Transactions on, vol. 26, pp. 308-318, 2011.
[14] U. Kamnarn and V. Chunkag, "Analysis and Design of a Modular Three-Phase AC-to-DC Converter Using CUK Rectifier Module With Nearly Unity Power Factor and Fast Dynamic Response," Power Electronics, IEEE Transactions on, vol. 24, pp. 2000-2012, 2009.
[15] M. G. Molina and P. E. Mercado, "A new control strategy of variable speed wind turbine generator for three-phase grid-connected applications," presented at the Transmission and Distribution Conference and Exposition: Latin America, 2008 IEEE/PES, 2008.
[16] O. Carranza, E. Figueres, G. Garcera, L. G. Gonzalez, and F. Gonzalez-Espin, "Peak Current Mode Control of a Boost Rectifier with Low Distortion of the Input Current for Wind Power Systems based on Permanent Magnet Synchronous Generators," presented at the Power Electronics and Applications, 2009. EPE '09. 13th European Conference on, 2009.
[17] Y. Xia, K. H. Ahmed, and B. W. Williams, "A New Maximum Power Point Tracking Technique for Permanent Magnet Synchronous Generator Based Wind Energy Conversion System," Power Electronics, IEEE Transactions on, vol. 26, pp. 3609-3620, 2011.
[18] X. Yuanye, K. H. Ahmed, and B. W. Williams, "Wind Turbine Power Coefficient Analysis of a New Maximum Power Point Tracking Technique," Industrial Electronics, IEEE Transactions on, vol. 60, pp. 1122-1132, 2013.
[19] X. Changliang, G. Qiang, G. Xin, S. Tingna, and S. Zhanfeng, "Input–Output Feedback Linearization and Speed Control of a Surface Permanent-Magnet Synchronous Wind Generator With the Boost-Chopper Converter," Industrial Electronics, IEEE Transactions on, vol. 59, pp. 3489-3500, 2012.
[20] O. Carranza, E. Figueres, G. Garcera, and R. Ortega, "Comparison of current control for low harmonic distortion applied to a small wind generation system with permanent magnet synchronous generator," presented at the IECON 2012 - 38th Annual Conference on IEEE Industrial Electronics Society, 2012.
[21] R. Itoh and K. Ishizaka, "Three-phase flyback AC-DC convertor with sinusoidal supply currents," Electric Power Applications, IEE Proceedings B, vol. 138, pp. 143-151, 1991.
[22] C. T. Pan and T. C. Chen, "Step-up/down three-phase AC to DC convertor with sinusoidal input current and unity power factor," Electric Power Applications, IEE Proceedings -, vol. 141, pp. 77-84, 1994.
[23] E. H. Ismail and R. Erickson, "Single-switch 3φ PWM low harmonic rectifiers," Power Electronics, IEEE Transactions on, vol. 11, pp. 338-346, 1996.
[24] J. Yungtaek and R. W. Erickson, "New single-switch three-phase high power factor rectifiers using multi-resonant zero current switching," presented at the Applied Power Electronics Conference and Exposition, 1994. APEC '94. Conference Proceedings 1994., Ninth Annual, 1994.
[25] B. Wu, High-Power Converters and AC Drives: Wiley, 2006.
[26] R. W. Erickson and D. Maksimovic, Fundamentals of Power Electronics: Springer, 2001.
[27] D. G. Holmes and T. A. Lipo, Pulse Width Modulation for Power Converters: Principles and Practice: John Wiley & Sons, 2003.
[28] M. Tomasini, R. Feldman, P. Wheeler, and J. C. Clare, "Input filter pre-charge scheme for high-power PWM-current source rectifiers connected to a weak utility supply," Power Electronics, IET, vol. 5, pp. 215-220, 2012.